Macromolecules 1989, 22, 2750–2755

Block Copolymers with Rigid and Flexible Segments

Klaus Huber*

Institut für Makromolekulare Chemie der Universität Freiburg, Stefan—Meier Strasse 31, D-7800 Freiburg, FRG. *Received August 12, 1988; Revised Manuscript Received November 22, 1988*

ABSTRACT: Some conformational properties of various block copolymers are investigated. In all cases the polymer consists of a rigid rod and two completely flexible blocks. Theoretical expressions are presented for the particle scattering function, the mean-square radius of gyration, and the hydrodynamic radius. The results are used to discuss the effect of combining in single copolymer segments, which are completely different in their flexibility.

Introduction

A simple and powerful model to describe polymers in solution is based on Gaussian statistics.[1] A more realistic model, which includes chain stiffness, is that of the persistence chain by Kratky and Porod.[2] Here a continuously bent thread describes the polymeric chain properties down to very low molecular weights. Chain flexibility (or chain stiffness) of both models is homogeneous along the contour of the molecule, a feature which is common to many polymers so far investigated.

There is, however, some evidence for the existence of biopolymeric molecules with blocks that differ significantly in their flexibility as for instance fibrinogen.[3] Another example is a single helix in the region of helix to coil transition, which recently was treated theoretically in terms of rods jointed by flexible coil segments.[4] Also polymer chemists are presently trying to modify thermodynamic behavior of rodlike molecules by introducing flexible side chains.[5] In such cases, the application of one homogeneous flexible chain model to both blocks can no longer be justified.

The present paper deals with a simple model for such heterogeneous polymers. Here, flexible chains are attached to a rodlike segment, and geometric as well as dynamic properties of cyclic and open conformers are calculated. In the cyclic conformer, the end-to-end distance of the flexible chain is fixed at a certain length, determined by the rodlike segment to which it is attached. This makes it possible to study the effect of geometric constraints on the structure within the polymer.

The Model

The model is composed of three segments: $2M + 1$ monomers, jointed by fixed bonds of length a, form a rodlike array of total length L. The flexible parts of the model are linear Gaussian chains, attached to both ends of the rod. Each Gaussian chain consists of N monomeric units of rms length b. This open structure (OS) can be considered as a special case of the Muroga treatment.[4] In addition, two further conformations are discussed in the following sections (see Figure 1): (i) In the cyclic structure, the two flexible parts are connected at the freely dangling ends, forming a closed loop (CS); (ii) the freely moving ends of the flexible chains are fixed at the center of the rod, i.e. at the monomeric unit of index $M + 1$, forming a twisted lemniscatelike shape (TS).

By starting with the distance distribution within the molecule, analytical expressions can be derived for the following quantities: (I) the mean-square distance between monomers k and l, $\langle R_{kl}^2 \rangle$, (II) the average interference factor from waves scattered by monomers k and l, $\langle \sin(qR_{kl})/(qR_{kl}) \rangle$, and (III) the average reciprocal separation of the monomer pair k and l, $\langle 1/R_{kl} \rangle$. These quantities are required for calculating the mean-square radius of gyration $\langle S^2 \rangle$, the particle scattering function $P(q)$ of the molecule, and the hydrodynamic radius R_h, all of which are accessible by scattering experiments. Here, q is the value of the scattering vector

$$q = (4\pi/\lambda) \sin(\theta/2) \tag{1}$$

with λ the wavelength in the medium and θ the scattering angle.

Some of the integrals occurring in the following sections are taken from tabulations of Gradshteyn and Ryzhik.[6]

Distance Distributions

The pair combinations of monomers within the molecule fall into different types, depending on the special conformer. The closed loop, denoted by CS, appears automatically as part of the treatment of the TS conformer and is not discussed separately in this section. In all cases, the x axis of the coordinate system is in the direction of the rod axis, and the distribution functions are separable into three independent Cartesian components.

OS Conformer. For the distance distribution of the OS conformer, four different types, schematically represented in Figure 2, have to be considered.

The first type, type A, comprises all pair combinations for which one monomer belongs to the rod and the other to the flexible chain; they are separated by n flexible and m rigid units and their distance is represented by the vector $\mathbf{R}_{kl}$, where $|l - k| = n + m$ and $R_{kl}^2 = X_{kl}^2 + Y_{kl}^2 + Z_{kl}^2$. The distribution function in the x direction results from a shift of origin by an amount $m \cdot a$, of the end-to-end distance within the flexible part:

$$w_A(X_{kl}) \sim \exp\{-(3/2b^2n)(X_{kl}^2 - 2X_{kl}ma + (ma)^2)\} \tag{2}$$

The distance distribution functions in the y and z direction are simply one-dimensional Gaussian distributions. Multiplication of all three parts leads to

$$w_A(R_{kl}) \sim \exp\{-(3/2b^2n)(R_{kl}^2 - 2R_{kl}ma \cos\vartheta + (ma)^2)\} \tag{3}$$

Here ϑ is the angle between $\mathbf{R}_{kl}$ and the rod axis. Integration over $\sin\vartheta \, d\vartheta$ and normalization finally results in

$$W_A(R_{kl}) = (3/2b^2n\pi)^{3/2} \exp\{-3(R_{kl}^2 + m^2a^2)/2b^2n\} \sinh\{3R_{kl}ma/b^2n\}(2nb^2/3maR_{kl}) \tag{4}$$

The second type, type B, combines monomers from the two flexible parts separated by the rod. Convolution of a one-dimensional Gaussian distribution with the distribution of eq 2, where m is substituted by $2M$, leads to the distribution function in the x direction. The distribution

* Present address: Ciba-Geigy AG, Division Farbstoffe und Chemikalien, CH-4002 Basel, Switzerland.

0024-9297/89/2222-2750$01.50/0

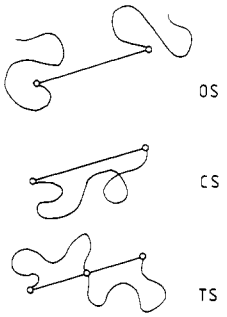

Figure 1. Schematic representation of the three block-copolymeric conformers: (OS) open structure, both flexible parts are equal in length; (CS) cyclic structure; (TS) twisted structure. The free ends of the two flexible blocks of the OS conformer are attached to the center of the rod. In all three cases, the model consists of $2M + 1$ rigid and $2N$ flexible monomers.

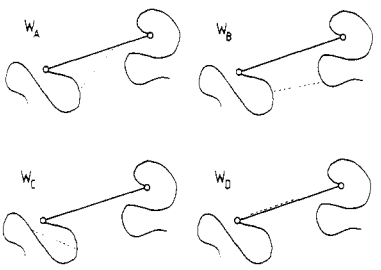

Figure 2. Types of pair combinations of monomers occurring in the OS conformer. The combinations are indicated by dashed lines.

functions in the other two directions are simply found by convolution of two one-dimensional Gaussian distributions. The result in three dimensions is

$$w_B(R_{kl}) \sim \exp\{-[3/2b^2(n_1 + n_2)](R_{kl}^2 - 2L(R_{kl}\cos\vartheta) - n_2L^2/n_1)\} \quad (5)$$

Here, n_1 and n_2 are the numbers of monomers of the two flexible parts, respectively, and L denotes the rod length. Integration over $\sin\vartheta\ d\vartheta$ and normalization leads to

$$W_B(R_{kl}) = \left(\frac{3}{2b^2(n_1 + n_2)\pi}\right)^{3/2} \exp\left\{-\left(\frac{3(R_{kl}^2 + L^2)}{2b^2(n_1 + n_2)}\right)\right\} \times \sinh\left\{\frac{3R_{kl}L}{b^2(n_1 + n_2)}\right\}\left(\frac{2(n_1 + n_2)b^2}{3LR_{kl}}\right) \quad (6)$$

Type C corresponds to the distribution function within an isolated Gaussian chain, and type D comprises the fixed distances within the rod.

TS Conformer. The interparticle distribution function has the general form

$$w(\mathbf{R}_{kl}) = \int \prod_{j=1}^{k-1} \tau_j(\mathbf{r}_j)\, d\mathbf{r}_j \times \int \prod_{j=k}^{l} \tau_j(\mathbf{r}_j)\delta(\sum_{j=k}^{l}\mathbf{r}_j - \mathbf{R}_{kl})\, d\mathbf{r}_j \int \prod_{j=l+1}^{N_T} \tau_j(\mathbf{r}_j)\, d\mathbf{r}_j \quad (7)$$

Here, the distribution function for the vector $\mathbf{R}_{kl}$ between the kth and the lth element of a molecule has been written by using Chandrasekhar's method[7] where $\delta(\sum_{j=k}^{l}\mathbf{r}_j - \mathbf{R}_{kl})$ is the Dirac δ function

$$\delta(\sum_{j=k}^{l}\mathbf{r}_j - \mathbf{R}_{kl}) \sim \int_{-\infty}^{+\infty} \exp\{-i\rho(\sum_{j=k}^{l}\mathbf{r}_j - \mathbf{R}_{kl})\}\, d\rho \quad (8)$$

$\tau_j(\mathbf{r}_j)$ is the distance distribution within the jth monomeric unit and N_T is the total number of monomers in the molecule.

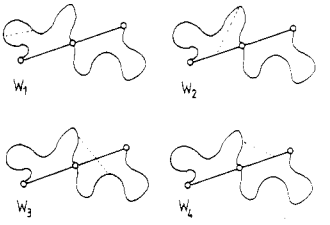

Figure 3. Types of pair combinations occurring in the TS conformer where flexible monomers are involved. The combinations are indicated by dashed lines.

Again the x axis is identical with the rod. To find the distribution function along this axis, the following procedure is applied: The rod will be introduced by $2M$ consecutive δ functions of the form $\delta(r_j - a)$. In the flexible part, three intraparticle distances $R_{1,N}$, $R_{N+1,2N}$, and $R_{1,2N}$ have to be fixed. However, since the rod axis coincides with the x axis, only two additional δ functions are introduced in eq 7, namely $\delta(R_{1,N} - Ma)$ and $\delta(R_{1,2N} - 2Ma)$. For further details the reader is referred to the Appendix.

As y and z components either the distribution functions of unperturbed Gaussian rings[8-11] or convolutions of such functions are used, depending on whether we are looking at distances within the same flexible part or distances between monomers of the two different flexible parts.

This time, the pair-distance distribution has to be grouped into five different functions, the distances for which are shown in Figure 3.

The first type, denoted as W_1, describes the distances within a flexible chain. It is worth mentioning that the same parameter μ occurs as in the flexible ring molecule[10]

$$\mu = n(1 - n/N) \quad (9)$$

W_2 combines rigid monomers with flexible monomers of the same loop.

The third type connects flexible units of both loops. The ring parameter μ has to be changed to

$$\mu' = n(1 - n/2N) \quad (10)$$

where the prime is used to distinguish it from the expression in eq 9. As an additional simplification, the parameter ν

$$\nu = 2\mu'N/(2\mu'N - (l + k - 2N)^2) \quad (11)$$

is introduced. Here, k and l are the indices of the two flexible units, which are the end points of vector $\mathbf{R}_{kl}$.

The fourth type, indicated as W_4, combines rigid monomers of one loop with flexible monomers of the other loop.

Type 5 is identical with type D of the OS conformer and represents the situation along the rod.

The distribution functions of all conformers, in which rigid monomers are combined with flexible ones, can be represented by the following expression

$$W(R) = 2\left(\frac{\beta}{\pi}\right)^{3/2} \exp\{-\gamma^2/4\beta\} \exp\{-\beta R^2\} \frac{\sinh\{\gamma R\}}{\gamma R} \quad (12)$$

The actual distribution functions are obtained by inserting the appropriate expressions for β and γ from Table I. As can be seen from this table, β stems from the flexible chain of the model and γ reflects the influence of the rigid rod.

Obviously, the distribution of eq 12 is no longer Gaussian but is modified by a factor $\sinh(\gamma R)/(\gamma R)$. In the limit of an infinitely small rod, γ is zero and

$$\lim_{\gamma \to 0} \sinh(\gamma R)/(\gamma R) = 1 \quad (13)$$

Equation 12 reduces to a common Gaussian distribution function, multiplied by a factor 2. This factor stems from the averaging over $\sin \vartheta \, d\vartheta$. Using actual values for β at $L = 0$, it is easily shown that W_1 passes into the Gaussian ring distribution[8-11] and W_3 assumes the Fukatsu–Kurata expression[12] for a Gaussian "lemniscate".

Averaged Geometric and Hydrodynamic Properties

In the case of $W_C(R)$, $W_D(R)$, and $W_5(R)$, the particle scattering function and the inverse first and second moments of the distribution functions are either trivial or well established.[13,14] For all other types of pair combinations, the distribution $W(R)$ of eq 12 has to be used.

In order to calculate the mean reciprocal distance and the mean-squared distance, the respective quantities have to be averaged over all possible orientations and distances, i.e. over the polar coordinates of the molecular fixed frame. Since the distribution function of eq 12 is already averaged over all $\sin \vartheta \, d\vartheta$, the remaining integral is just over $d\varphi R^2 \, dR$.

For the calculation of the average interference factor, the reference frame used is now the laboratory-fixed coordinate system with the polar axis along the vector **q**.

Interference Factor. The interference factor of monomers k and l is defined as

$$P_{kl}(q) = 4\pi \int_0^\infty W(R_{kl}) R_{kl}^2 \sin(qR_{kl})/(qR_{kl}) \, dR_{kl} \quad (14)$$

Replacing $W(R_{kl})$ by $W(R)/2$ from eq 12 and substituting this function into eq 14, one finds

$$P_{\beta\gamma}(q) = 4\pi \int_0^\infty dR \left(\frac{\beta}{\pi}\right)^{3/2} \exp\{-\gamma^2/4\beta\} \times \exp\{-\beta R^2\} \frac{\sinh\{\gamma R\}}{q\gamma} \sin(qR) \quad (15)$$

This integral can be solved analytically to yield

$$P_{\beta\gamma}(q) = \frac{\sin(q\gamma/2\beta)}{(q\gamma/2\beta)} \exp\{-q^2/4\beta\} \quad (16)$$

as the pair interference factor. The actual values for β and γ of the corresponding types of pair combinations again can be taken from Table I.

Inverse First Moment. The mean reciprocal distance $\langle 1/R_{kl} \rangle$ between two monomers k and l is defined as follows:

$$\langle 1/R_{kl} \rangle = \int_0^\infty (1/R_{kl}) W(R_{kl}) 2\pi R_{kl}^2 \, dR_{kl} \quad (17)$$

Inserting eq 12, this equation becomes

$$\langle 1/R \rangle_{\beta\gamma} = 2\pi \int_0^\infty dR \, 2\left(\frac{\beta}{\pi}\right)^{3/2} \exp\{-\gamma^2/4\beta\} \exp\{-\beta R^2\} \frac{\sinh\{\gamma R\}}{\gamma} \quad (18)$$

This integral can be represented in two different ways:[15]

$$\langle 1/R \rangle_{\beta\gamma} = \frac{4\beta}{\sqrt{\pi}\gamma} \int_0^{(\gamma/2\sqrt{\beta})} e^{-t^2} \, dt = 2\frac{\beta}{\gamma} \operatorname{erf}(\gamma/2\sqrt{\beta}) \quad (19a)$$

$$\langle 1/R \rangle_{\beta\gamma} = 2(\beta/\pi)^{1/2} \exp\{-\gamma^2/4\beta\} \phi\{1,3/2;(\gamma^2/4\beta)\} \quad (19b)$$

In eq 19a erf stands for the tabulated error function,[15] and

Table I
Parameters β and γ from Equation 12

conformer	type of combination	β	γ
OS	W_A	$3/2nb^2$	$3ma/nb^2$
OS	W_B	$3/2(n_1 + n_2)b^2$	$6Ma/(n_1 + n_2)b^2$
TS	W_1	$3/2\mu b^2$	$3nMa/N\mu b^2$
TS	W_2	$3/2\mu b^2$	$3(nM - Nm)a/N\mu b^2$
TS	W_3	$3\nu/2\mu' b^2$	$3\nu nMa/N\mu' b^2$
TS	W_4	$3/2\mu b^2$	$3(nM + Nm)a/N\mu b^2$

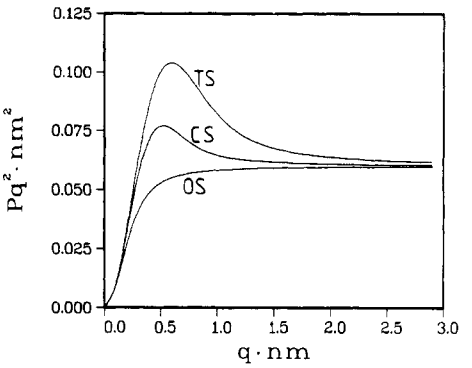

Figure 4. Kratky plots of the particle scattering functions in the ideally flexible limit, i.e. at zero rod length: (TS) twisted ring, (CS) regular ring, (OS) linear coil. All three models consist of 200 Gaussian monomers with an averaged length $b = 1$ nm.

ϕ of eq 19b denotes a degenerate hypogeometric series. Values for $\langle 1/R \rangle_{\beta\gamma}$ can now be calculated numerically.[16]

Squared Intraparticle Distance. For the intraparticle distances, the following integral is obtained

$$\langle R^2 \rangle_{\beta\gamma} = 2\pi \int_0^\infty dR \, R^4 2\left(\frac{\beta}{\pi}\right)^{3/2} \exp\{-\gamma^2/4\beta\} \exp\{-\beta R^2\} \frac{\sinh\{\beta R\}}{\beta R} \quad (20)$$

Equation 20 can again be represented in terms of a degenerate hypogeometric series.[15] An alternative derivation of $\langle R^2 \rangle_{\beta\gamma}$, which leads to a closed expression, follows from a series expansion of the pair interference factor.

$$\left\langle \frac{\sin(qR)}{(qR)} \right\rangle_{\beta\gamma} = \frac{\sin(q\gamma/2\beta)}{(q\gamma/2\beta)} \exp\{-q^2/4\beta\} \quad (21)$$

Taylor series expansion on both sides yields

$$\langle 1 - q^2R^2/6 + \ldots \rangle_{\beta\gamma} = (1 - q^2(\gamma/2\beta)^2/6 + \ldots)(1 - q^2(1/4\beta)/6 + \ldots) \quad (22)$$

Collection of all coefficients to q^2 and comparison of both sides of eq 22 leads to

$$\langle R^2 \rangle_{\beta\gamma} = (\gamma/2\beta)^2 + (1/4\beta) \quad (23)$$

Discussion

Particle Scattering Function. In order to obtain the scattering function of the three conformers, the integral of eq 16 over all combinations of $n + m$ monomers has to be evaluated. This cannot be done analytically for most types of pair combinations. Therefore, numerical methods have here been used, which in the case of the particle scattering factor consists of a single integration.[16]

Figure 4 shows the scattering behavior of the completely flexible structures, obtained from the three conformers at $L = 0$. The OS conformer becomes a linear Gaussian chain[13] represented by curve OS. Curve CS corresponds to the Gaussian ring,[9] and curve TS is the scattering curve

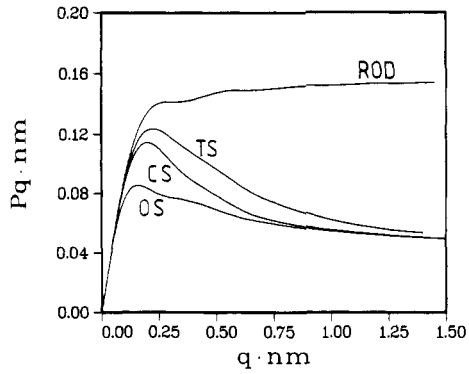

Figure 5. Holtzer plot for the three conformers, TS, CS, and OS. The flexible part has the same size as in Figure 4. The rodlike part consists of 201 monomers of length 0.1 nm. The upper curve (ROD) corresponds to the pure rod.[21]

for a twisted Gaussian ring. All three chains have the same number of monomers. Recently, the Gaussian ring model[9] has been successfully applied to describe the scattering behavior of polystyrene ring molecules in a θ solvent.[17]

A common feature of all models obeying Gaussian chain statistics is that $P(q)$ goes with q^{-2} in the high q limit. Therefore, the scattering curves are represented as $q^2P(q)$ vs q often referred to as Kratky plots. Molecules with segment densities higher than in linear Gaussian chains, like stars or rings, pass through a maximum before reaching the plateau region. Obviously, this maximum is more pronounced if the ring is twisted to a lemniscatelike shape. Hence, Kratky plots should help to distinguish between simple and twisted rings.

Figure 5 represents the scattering functions of the same conformers if a rodlike segment is introduced. Scattering functions of molecules, which are either semiflexible or rigid, show typical q^{-1} behavior at large q values. This suggests a plot of $P(q)\cdot q$ versus q (Holtzer plot) rather than $P(q)\cdot q^2$. Then again plateau values exist where $\lim_{q\to\infty} P(q)\cdot q = \pi/L$; i.e., the height of the plateau is proportional to the inverse contour length[18] of the rigid and semiflexible chain. If parts of the molecule are Gaussian, they do not contribute to this plateau value. In the present model, this leads to a decrease of the plateau height by a factor of $(2M + 1)^2/(2N + 2M + 1)^2$ relative to the corresponding rigid rod. This decrease can be expected to be less pronounced if the more flexible part is wormlike instead of completely flexible.

In Figure 6 the scattering behavior is investigated for different statistical segment lengths b at constant contour length of the flexible part as well as of the rod. In order to retain the influence of the rodlike segment, the ratio N/M is kept constant. The qualitative behavior is the same for all three conformers. A decrease of the maximum in the Holtzer plot is observed if the number of flexible monomers at constant contour length is decreased. The rms distance $\langle R_t^2\rangle^{1/2}$ between end points of a contour section t increases if b is increased at constant $t = nb$, and it modifies the scattering behavior only at low and medium q values.

Hydrodynamic Radius. According to the theory of Kirkwood and Riseman,[14] the hydrodynamic radii can be calculated by integrating eq 19 over all pair combinations of monomers. Again, this can only be done by numerical integration.[16] For the homogeneous parts, i.e. the rigid rod and the linear and cyclic Gaussian chain, the integrals are known from the literature.[19,14,20] It has to be borne in mind that $\langle 1/R\rangle$ diverges if one of the monomeric lengths a or b becomes very small. In order to avoid physically meaningless results, the monomers are assumed not to

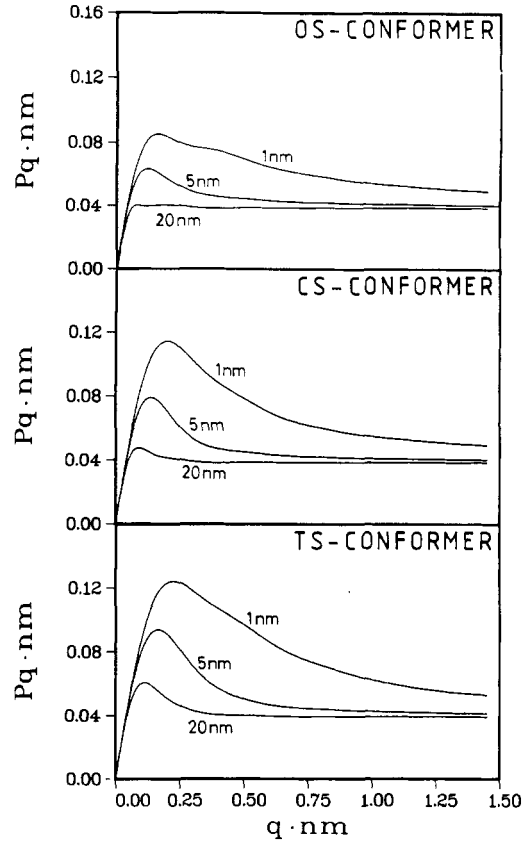

Figure 6. Holtzer plots at three different lengths for the flexible monomer b (1, 5, and 20 nm). The overall contour length of the flexible part is kept constant at 200 nm and the one of the rod at 20 nm.

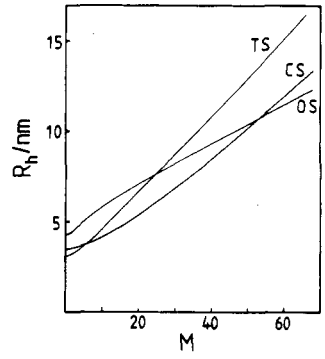

Figure 7. Hydrodynamic radii as a function of the rod length L at constant size of the flexible part Nb = 100 nm. Both monomeric units have the same length $a = b$ = 1 nm.

differ in length and the monomer length was used as a cutoff parameter in integrating eq 19.

In Figure 7, hydrodynamic radii are plotted as a function of the rod length, $L = 2Ma$, for all three conformers. The size of the flexible chains, Nb, is kept constant and $a = b$ = 1.0 nm. For very small rod length, the behavior is regular in that $R_h(\mathrm{OS}) > R_h(\mathrm{CT}) > R_h(\mathrm{TS})$. If the rod length increases beyond the range of the end-to-end distances for the corresponding free flexible chains, i.e. $M > 10$, the results become pathological. Namely, $R_h(\mathrm{TS})$ and $R_h(\mathrm{CS})$ exceed $R_h(\mathrm{OS})$. An increasing rod extends the end-to-end distance of the flexible chains. This in turn leads to an increase of intramolecular distances within the flexible chains. Such distances are of small or medium magnitude in the undeformed state, and the effect of stretching is more pronounced on R_h than on $\langle S^2\rangle$, as will be seen in the following sections.

Mean-Square Radius of Gyration. For the mean-

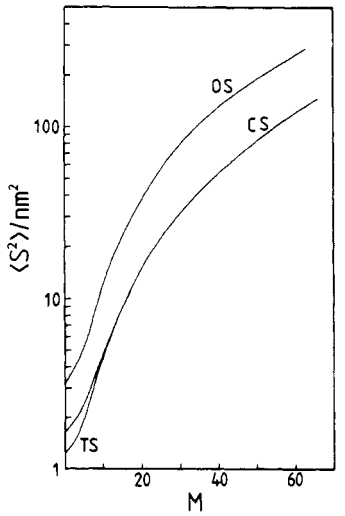

Figure 8. Mean-square radius of gyration at varying rod lengths L. The same parameters are used as in Figure 7.

square radius of gyration an analytical expression can be given for all three conformers:

OS conformer

$$\langle S^2\rangle_{OS} = 1/(2M + 2N)^2[4M^2N^2a^2 + 4N^3b^2/3 + 16NM^3a^2/3 + 2MN^2b^2 + 4M^4a^2/3] \quad (24)$$

CS conformer

$$\langle S^2\rangle_{CS} = 1/(2M + 2N)^2[4M^2N^2a^2/3 + 2N^3b^2/3 + 8NM^3a^2/3 + 4MN^2b^2/3 + 4M^4a^2/3] \quad (25)$$

TS conformer

$$\langle S^2\rangle_{TS} = 1/(2M + 2N)^2[4M^2N^2a^2/3 + N^3b^2/2 + 8NM^3a^2/3 + 2MN^2b^2/3 + 4M^4a^2/3] \quad (26)$$

The derivation of these expressions is based on eq 23 and on the corresponding equations of a linear Gaussian chain and a rigid rod. Figure 8 shows a plot of $\langle S^2\rangle$ at varying rod length for all three conformers. The same parameters are used as in Figure 7. For $L = 0$, correct answers are obtained corresponding to a linear, cyclic, and twisted Gaussian chain. The g ratio defined as

$$g_{CS} = \langle S^2\rangle_{CS}/\langle S^2\rangle_{OS} \quad (27a)$$

$$g_{TS} = \langle S^2\rangle_{TS}/\langle S^2\rangle_{OS} \quad (27b)$$

approaches the value $^1/_2$ for the CS conformer and $^3/_8$ for the TS conformer as were previously calculated for cyclic[8] and twisted Gaussian rings.[12]

For low rod lengths, the size of the CS conformer lies between the OS and TS conformers, as expected. At rod lengths with M larger than 20, the curve of the TS conformer merges with that of the CS conformer because they approach the rod structure. The curves of all three conformers coincide only for $M > 10^3$.

Concluding Remarks. Two final comments are necessary: (i) It is self-evident that for values of $L/2 > Nb$, the CS and TS conformers no longer have a physical meaning. In a real polymer chain, the end-to-end distance cannot exceed its contour length. (ii) Even for a certain region of L around or below Nb, the theoretical results have to be treated with caution, because in the present model the distributions in y and z directions are not changed during the increase of the end-to-end distance in the x direction. If the elongation ratio is high enough, the application of Gaussian statistics is no longer justified.

Acknowledgment. The idea for this work was developed during a very stimulating discussion with Professor Burchard about the structure of fibrinogen. I express my gratitude to Professor Burchard and to Professor Stockmayer for many helpful comments. This work was supported by the Deutsche Forschungsgemeinschaft within the scheme of SFB 60.

Appendix: Derivation of W_3

The distribution function $W_3(R_{kl})$ is used to represent the derivation procedure for the TS conformer in more detail. Here, the vector $\mathbf{R}_{kl}$ connects the flexible monomer of index k on one loop with the lth monomer on the other loop. Let

$$n = l - k \quad (A1)$$

$$R_{kl}^2 = X_{kl}^2 + Y_{kl}^2 + Z_{k_l}^2 \quad (A2)$$

$$r_j^2 = x_j^2 + y_j^2 + z_j^2 \quad (A3)$$

where X_{kl}, Y_{kl}, Z_{kl} and x_j, y_j, z_j are the Cartesian components of the end-to-end vector $\mathbf{R}_{kl}$ and the bond vector $\mathbf{r}_j$, respectively.

The starting equation is eq 7, which becomes for w_3

$$w_3(X_{kl}) \sim \int_{-\infty}^{+\infty} d\rho \int_{-\infty}^{+\infty} d\sigma \int_{-\infty}^{+\infty} d\kappa \exp\{-i\sigma X_{kl}\} \times \exp\{-i\kappa L/2\} \exp\{-i\rho L\} \int \prod_{j=1}^{k} \tau_j \exp\{i(\rho + \kappa)x_j\}\, dx_j \times \int \prod_{j=k+1}^{N} \tau_j \exp\{i(\rho + \kappa + \sigma)x_j\}\, dx_j \int \prod_{j=N+1}^{l} \tau_j \times \exp\{i(\rho + \sigma)x_j\}\, dx_j \int \prod_{j=l+1}^{2N} \tau_j \exp\{i\rho x_j\}\, dx_j \quad (A4)$$

The distribution under consideration is in the x direction, which corresponds to the rod axis. The distance distribution of the jth monomeric unit in one dimension has the following form

$$\tau_j = (3/2\pi b^2)^{1/2} \exp\{-3x_j^2/2b^2\} \quad (A5)$$

which is independent of the index j. Integration over all x_j gives

$$w_3(X_{kl}) \sim \int_{-\infty}^{+\infty} dU \int_{-\infty}^{+\infty} dQ \int_{-\infty}^{+\infty} dV \exp\left\{-i\frac{\sqrt{6}}{b}[VX_{kl} + QL/2 + UL]\right\} \exp\{-k(U + Q)^2\} \exp\{-(N - k)(U + Q + V)^2\} \exp\{-(l - N)(U + V)^2\} \exp\{-(2N - l)U^2\} \quad (A6)$$

where the following replacements have been made

$$\rho^2 = 6U^2/b^2 \quad (A7)$$

$$\sigma^2 = 6V^2/b^2 \quad (A8)$$

$$\kappa^2 = 6Q^2/b^2 \quad (A9)$$

After integration over U, Q, and V, eq A6 becomes

$$w_3(X_{kl}) \sim \exp\left\{-\frac{3}{2b^2\mu'}\left[\frac{\mu' L^2}{2N} + \frac{2N\mu'}{2\mu' N - (l + k - 2N)^2}\left(\frac{nL}{2N} - X_{kl}\right)^2\right]\right\} \quad (A10)$$

The distribution functions of the y and z component are convolutions of one-dimensional distribution functions

from regular Gaussian rings.[8-11] After multiplying of all three components, one obtains

$$w_3(R_{kl}) \sim \exp\left\{-\frac{3}{2b^2\mu'}\left[\frac{\mu' L^2}{2N} + \frac{2N\mu'}{2\mu' N - (l+k-2N)^2}\left(\frac{L^2 n^2}{4N^2} - \frac{n}{N} L R_{kl} \cos\vartheta + R_{kl}^2\right)\right]\right\} \quad \text{(A11)}$$

Averaging over all $\sin\vartheta\, d\vartheta$ and using ν from eq 11 leads to

$$W_3(R_{kl}) \sim \exp\left\{-\frac{3}{2b^2\mu'}\left[\frac{\mu' L^2}{2N} + \frac{\nu n^2 L^2}{4N^2} + \nu R_{kl}^2\right]\right\} \times 2\frac{\sinh\{3\nu n L R_{kl}/2N\mu' b^2\}}{3\nu n L R_{kl}/2N\mu' b^2} \quad \text{(A12)}$$

Normalization of eq A12 over $d\varphi R_{kl}^2\, dR_{kl}$ finally results in

$$W_3(R_{kl}) = 2\left(\frac{3\nu}{2b^2\pi\mu'}\right)^{3/2} \exp\left\{-\frac{3L^2\nu n^2}{8b^2N^2\mu'}\right\} \exp\left\{-\frac{3\nu R_{kl}^2}{2b^2\mu'}\right\} \times \frac{\sinh\{3L\nu n R_{kl}/2b^2 N\mu'\}}{(3L\nu n R_{kl}/2b^2 N\mu')} \quad \text{(A13)}$$

References and Notes

(1) Lord Rayleigh *Philos. Mag.* **1919**, *37*, 321.
(2) Kratky, O.; Porod, G. *Recl. Trav. Chim. Pays-Bas* **1949**, *68*, 1106.
(3) Doolittle, R. F. *Annu. Rev. Biochem.* **1984**, *53*, 195, references therein.
(4) Muroga, Y. *Macromolecules* **1988**, *21*, 2751.
(5) Wenzel, M.; Ballauff, M.; Wegner, G. *Makromol. Chem.* **1987**, *188*, 2865.
(6) Gradshteyn, I. S.; Ryzhik, I. M. *Table of Integrals, Series, and Products*; Academic Press: New York, San Francisco, London, 1965.
(7) Chandrasekhar, S. *Rev. Mod. Phys.* **1943**, *15*, 1.
(8) Zimm, B.; Stockmayer, W. H. *J. Chem. Phys.* **1949**, *17*, 1301.
(9) Casassa, E. F. *J. Polym. Sci., Part A* **1965**, *3*, 605.
(10) Yamakawa, H. *Modern Theory of Polymer Solutions*; Harper & Row: New York, Evanston, San Francisco, London, 1971; Sec. 9b.
(11) Burchard, W. In *Cyclic Polymers*, Semlyen, J. A. Ed.; Elsevier: London, 1986; Chapter 2.
(12) Fukatsu, M.; Kurata, M. *J. Chem. Phys.* **1966**, *44*, 4539.
(13) Debye, P. In *Light Scattering from Dilute Polymer Solutions*; McIntyre, D., Eds.; Gormick, F., Eds.; Gordon and Breach: New York, London, 1964; p 139.
(14) Kirkwood, J. G.; Riseman, J. *J. Chem. Phys.* **1948**, *16*, 565.
(15) Abramowitz, M.; Stegun, I. A. *Handbook of Mathematical Functions*; Dover: New York, p 295.
(16) Numerical calculations were performed with subprograms of the *IMSL LIBRARY* and *IMSL SFUN/LIBRARY*, IMSL, Inc., Houston, TX, 1985.
(17) Hadziioannou, G.; Cotts, P. M.; ten Brinke, G.; Han, C. C.; Lutz, P.; Strazielle, P.; Rempp, P.; Kovacs, A. J. *Macromolecules* **1987**, *20*, 493.
(18) Schmidt, M.; Paradossi, G.; Burchard, W. *Macromol. Chem. Rapid Commun.* **1985**, *6*, 767.
(19) Riseman, J.; Kirkwood, J. G. *J. Chem. Phys.* **1950**, *18*, 512.
(20) Bloomfield, V. A.; Zimm, B. *J. Chem. Phys.* **1966**, *44*, 315.
(21) Neugebauer, T. *Ann. Phys.* **1943**, *42*, 509.

Quasi-Elastic and Electrophoretic Light Scattering Studies of the Reorganization of Dioleoylphosphatidylcholine Vesicle Membranes by Poly(2-ethylacrylic acid)

Ki Min Eum,[†] Kenneth H. Langley,*[,†] and David A. Tirrell[‡]

Departments of Physics and Astronomy and Polymer Science and Engineering, University of Massachusetts, Amherst, Massachusetts 01003.

Received May 2, 1988; Revised Manuscript Received December 16, 1988

ABSTRACT: Quasi-elastic light scattering (QELS) and electrophoretic light scattering (ELS) measurements have been used to investigate the pH-dependent structural reorganization of phospholipid vesicles suspended in aqueous solutions of poly(2-ethylacrylic acid) (PEAA). The average radius of dioleoylphosphatidylcholine (DOPC) vesicles suspended in aqueous PEAA was reduced within 1 h from approximately 600 to 60 nm upon acidification. Size distribution analysis revealed narrow single peaks far from the pH at which the reorganization occurs but bimodal distributions in the transition region. The transition pH was shifted from 7.0 to 6.5 as the ionic strength of the sample solutions was increased from 50 to 500 mM. The conformational transition of PEAA from an expanded form at high pH to a relatively compact coil in acidic solutions was also observed by QELS. ELS measurements showed that, as the pH is lowered from 8.0 to 5.5 in the presence of PEAA, the electrophoretic mobility of DOPC vesicles passes through a minimum at the transition pH. At pH lower than that of the transition, vesicle mobility is greater in PEAA solutions than in simple buffers. We believe the increase in mobility is due to adsorption of PEAA on the vesicle surface. We infer that as the pH is lowered, the collapsed PEAA chain provides a hydrophobic site for solubilization of the phospholipid hydrocarbon tails and in so doing disrupts the structural organization characteristic of the pure phospholipid.

Introduction

Surfactant bilayers have been a subject of intense scientific interest for the last 2 decades, since Bangham's[1] illustration of the analogy between such "liposomal" structures and the complex plasma membranes of cells. An essential and intriguing characteristic of the natural membranes is their capacity to respond to signals of various kinds; membrane signaling plays a critical role in intercellular communication, in the binding and processing of ligands and receptors, in energy transduction, and in many other vital cellular processes.

We have explored over the last several years a simple approach to the construction of synthetic bilayer membranes that share this essential capacity to respond to

[†] Department of Physics and Astronomy.
[‡] Department of Polymer Science and Engineering.

0024-9297/89/2222-2755$01.50/0